Solid State Phenomena *Online: 2014-09-26*
ISSN: 1662-9779, Vol. 219, pp 161-164
doi:10.4028/www.scientific.net/SSP.219.161

Fluid flow and defect density considerations when drying bumped wafers using spin and surface tension gradient methods

Daniel L. Goodman[a], Dustin Rabideau and Mani Sobhian

TEL-NEXX Inc., Billerica, MA 01821 USA

[a]Daniel.Goodman@us.tel.com

Keywords: Advanced packaging, bumped wafers, copper pillar, defect density, SRD, surface tension gradient, microfluidic channels, resist strip, wafer drying

INTRODUCTION

Spin rinse drying (SRD) and surface tension gradient drying (STG) are used to clean and dry wafers after wet processing. These methods are effective at removing surface fluid and fluid trapped by capillary forces in small (<1um) features. SRD and STG processes combine driven fluid flows with controlled evaporation of thin water films to leave a dry wafer with low defect density (i.e. a low number of physical particle process adders, or areas of haze or oxidation).

In advanced packaging, copper pillar bumps and other tall (30-150um) metal connection features are formed on the wafer to allow electrical and thermal connections to the substrate. These features can trap rinse fluid, making low defect-density drying more difficult. The standard process solution for both SRD and STG is to combine driven fluid flow with evaporative drying.

This paper presents a model for drying of wafers with tall features using either SRD or STG processes. The model predicts the portion of drying due to driven flow and due to evaporative drying. Understanding these relative contributions is useful for equipment design, process optimization and for interpreting defect density results. Predictions are compared with results of STG drying experiments and show general agreement.

DRYING MODEL

A spin rinse dry geometry is shown in Fig. 1. A chucked wafer of radius R_w is shown rotating at an angular velocity ω. A packaging connection feature of height h_0 is located at radius R_b. During a typical SRD process, water is injected at low flow (1-2 cm^3/s) during low velocity (ω ~10 rad/s) rotation. The water height is greater than the feature height h_0, so features are fully submerged, and flow to the edges is established. Water flow is discontinued as rotation velocity is increased to a maximum speed of 100-200 rad/s. The starting time for the SRD model is when the water level is equal to the feature height $h(t=0)=h_0$.

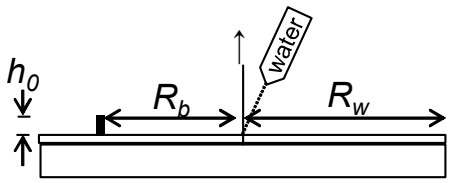

Figure 1: SRD model geometry.

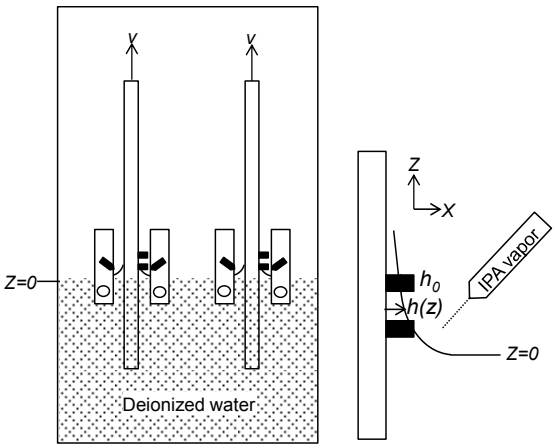

Figure 2: STG model geometry.

An STG geometry is shown in Fig. 2. Wafers are vertically pulled out of a deionized water bath at a slow (1-10mm/s) velocity *v*. Isopropyl alcohol (IPA) vapor is directed at the position where the wafer and water meet and form a meniscus. The capillary length $\lambda_c = (\Gamma/\rho g)^{1/2} = \sim 2mm$ which sets the meniscus dimension is much larger than the connection features (30-100um). The water height is $h(z)$, where z=0 is defined as the water surface height. The connection feature model

geometry is shown in Fig. 3. Cylinders of height h_0 and radius r are arranged on a rectangular grid with pitch spacing L_p. Fluid at a height h flows through the cell at volumetric rate Q (cm^3/s) during the drying process. The flow length L is assumed long compared to the unit, and so contains many unit cells ($L/L_p >> 1$). Both the SRD and STG generate forces which drive fluid flows. The SRD and STG pressures are:

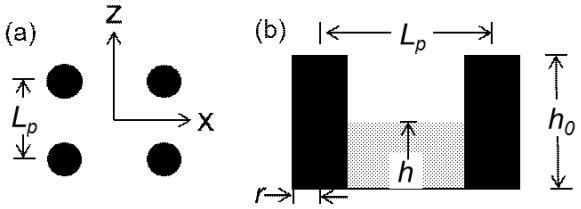

Figure 3: Connection feature model geometry.

$$\Delta p_{SRD} = \rho\omega^2 R_b,\ \Delta p_{STG} = d\Gamma/dz \cong \Delta\Gamma/\lambda_c \tag{1}$$

where $\Delta\Gamma$ is the difference between the IPA and water surface tensions. This is balanced by a resistance force exerted by the bumps during drying which can be characterized by a Fanning friction factor *f,* also known as a drag coefficient C_D [1]. For a characteristic kinetic energy $K = \rho v^2/2$, and wetted area A_w, the force F_k is:

$$F_k = KA_w f = K(A_{w1}f_1 + A_{w2}f_2) \tag{2}$$

The first friction term is due to direct friction with the front of the bumps. The second term is due to friction with the wafer surface as well as the sides of the bumps which confine of the fluid into flow channels. Calculation and measurement of fluid friction with a submerged cylinder is a problem with a long history [2,3]. A good fit to data in Ref. 4 in our low Reynolds number ($\mathrm{Re} = D_\perp v/\eta < 1$) flow regime is:

$$f_1 = (\sqrt{4.0/\mathrm{Re}} + 1.2)^2 \tag{3}$$

Pressure-driven flow through long, straight channels of constant cross-section with non-slip boundary conditions is referred to as Hagen-Poiseuille (or simply Poiseuille) flow. The channel is characterized by a hydraulic resistance:

$$R_{hyd} = \Delta p/Q = \alpha L\eta/A_\perp^2 \tag{4}$$

where $\eta = \mu/\rho$ is the kinematic viscosity and α is a geometrical correction factor. Correction factors α for a variety of micro-fluidic channel cross sectional shapes have been found by solving the Poisson equation for the velocity profile [4]. At low Reynolds number, the friction factor and hydraulic pressure approaches are equivalent with the relationship: $f = \dfrac{2\alpha}{\pi\,\mathrm{Re}}$. For a closed channel of width-to-height ratio $\gamma = w/h$, a closed-form solution for α is [4]:

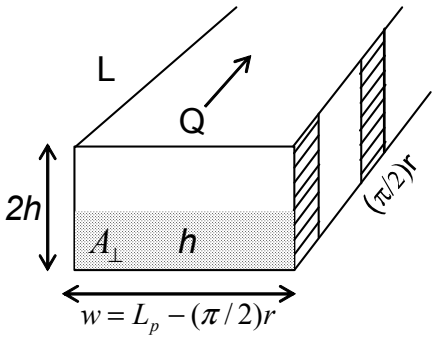

Figure 4: Poiseuille channel model with reduced width and sidewall areas consistent with bump dimensions of Fig. 3.

$$\alpha(\gamma) = \frac{\pi^3\gamma^2}{8}\left[\sum_{n=1,3,5,\ldots}^{\infty}\frac{n\gamma}{\pi\cdot n^5} - \frac{2}{\pi^2 n^5}\tanh(n\pi\gamma/2)\right]^{-1} \tag{5}$$

In the range of geometric interest, $1 < \gamma < 10$, a good fit to Eq. (4) is $\alpha(\gamma) = 16 + 10\gamma$. Using the symmetry of solutions to Poisson's equation for open and closed channels: $Q_o(w/h) = Q_c(w/2h)/2$, the flow in the open rectangular channel is:

$$Q_o(w/h) = \frac{2\Delta p w^2 h^3}{(16h + 5w)\eta L} \tag{6}$$

Combining Eqs. 2-6 and approximating Eq. 3 as $f_1 \approx 2/\mathrm{Re}$, we find a hydraulic resistance to flow in tall bumps in the Poiseuille regime:

$$\frac{\Delta p}{Q} = \frac{\eta L}{2}\left[\frac{1}{L_p r^2 h} + \frac{(ah+5w)}{w^2 h^3}\right] \qquad (7)$$

where the parameter $a(L_p, r)$ accounts for the reduced sidewall friction of a discontinuous channel and the effective channel width is *w,* both as shown in Fig 4. Using the definition for flow $Q(h,t) = A_c dh(t)/dt$ where the channel floor area per unit cell is $A_c = L_p^2 - \pi r^2$, and substituting SRD or STG driving pressures from Eq. 1, we integrate Eq. 6 to solve for *h(t).* The initial condition dh_0/dt is set by external flow for the SRD and by lift speed and the meniscus equation [5] for STG. The leading order term for small h is of the form: $h(t) \approx (1/h_0^2 + ct)^{-1/2}$, where $c \approx \Delta p/\eta L$. A typical solution for SRD drying using all the terms is shown in Fig. 5. A characteristic of these profiles is an initial rapid drop followed by a long tail. This non-linear behavior is due to the $1/h^3$ dependence of hydraulic resistance in a channel with large compactness ratio $C \equiv P^2/A$ where P is the wetted perimeter and A is the fluid cross-sectional area.

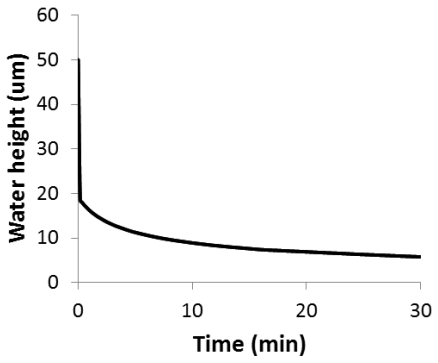

Figure 5: Predicted water height remaining between 50um bumps with 200um pitch during SRD drying at 100 rad/s without evaporation.

EXPERIMENTAL RESULTS

Photoresist from wafers with tall bump features ranging from 30-90 um and pitches ranging from 74-200um were stripped, rinsed and dried in an experimental resist strip tool at TEL-NEXX in Billerica, MA. The tool processes eight wafers in a parallel single wafer geometry which allows batch processing but the uniformity and process control characteristic of single wafer tools [6]. After high-rate stripping using shear-plate™ agitation, wafers were rinsed with deionized water and dried using Marangoni drying in an IPA vapor STG module. The drying module has an integrated manifold containing a DIW overflow weir and IPA vapor delivery system for simultaneously processing eight wafers. The drying system also contains a heating manifold above the IPA vapor delivery system for post-evaporative drying. Process parameters which were optimized included wafer lift speed, DIW temperature, post-evaporative drying temperature, IPA vapor flow and IPA vapor concentration in the N2 carrier gas. The IPA vapor concentration was set by adjusting the IPA liquid temperature in a N2 bubbler.

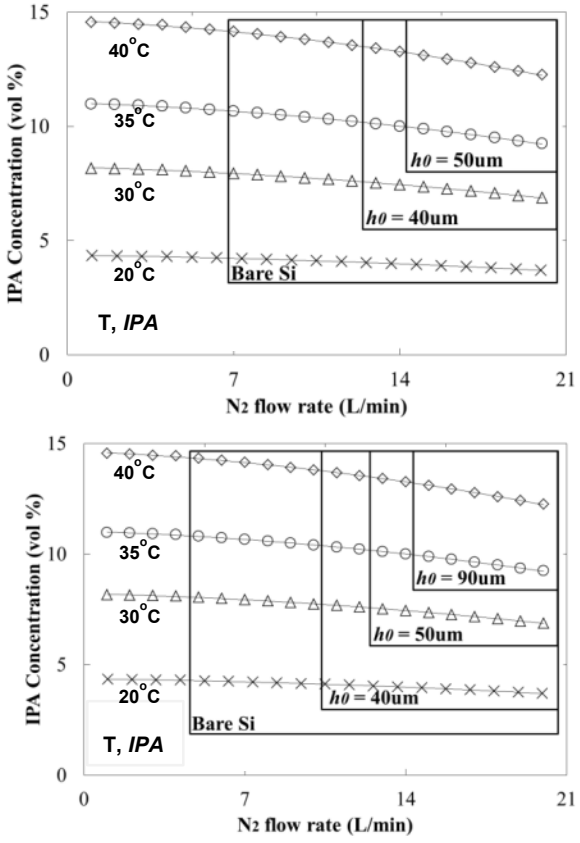

Figure 6: Process windows for STG drying post-evaporation: a) at 30°C for 150s by raising DIW temperauture, and b) at 60°C for 60s using a vertical heating plate manifold. N2 flow is total required to dry eight wafers simultaneously. Labelled curves are saturated equilibrium for IPA/N2 for IPA bubbler pressure and flow. See Table 1 for additional process and wafer parameters.

STG processing using room temperature DIW is effective at drying bare silicon wafers and bumps smaller than ~30um. Larger bumps required additional evaporative drying, either by raising the DIW temperature or using the heating plate manifold. The process window for STG processing is shown in Figs. 6 and 7 with data summarized in Table 1. A DIW temperature of 50°C produced a post-STG evaporative drying temperature of 30°C for 150s, and allowed full drying of wafers with up to 50um bump height. A wafer temperature of 60°C was sufficient post-processing evaporation to fully dry wafers with bump height of 90um.

Table 1: Wafer and process parameters to achieve dry wafers with STG processing.

Height h0 (um)	Pitch Lp (um)	Dia 2r (um)	F*m* Area Ratio	IPA Conc (%vol)	Total N2 flow (L/min)	Lift Speed (mm/2)	Post Evap (°C)	Evap Time (s)
0	NA	NA	0	4	5-9	1.5	20	0
40	190	120	0.52	4-7	9-15	1.5	30-60	60-150
50	190	120	0.65	7-10	15	1.5	30-60	60-150
90	190	120	1.17	10-13	15-21	1.5	60	150

In general, there will be a range of bump geometries on a wafer, with varying degrees of drying difficulty. The values for pitch in Table 1 are for the tightest features which are the most difficult to dry. Also listed in the table is a figure of merit (F_m) which can be used to compare wafer geometries to predict difficulty of drying. The figure of merit is the ratio of wetted bump area to wetted channel floor area:

$$F_m = \frac{2\pi r h_0}{L_p^2 - \pi r^2} \tag{8}$$

Geometries with large *FOM* will retain water between bumps and require additional evaporative drying.

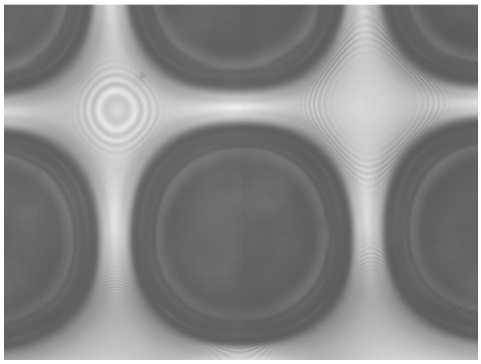

Figure 7: Trapped water between bumps of 50um height. Contours of constant height in the meniscus region are visible in the areas between bumps.

SUMMARY AND OBSERVATIONS

SRD and STG wafer processing combine driven fluid flow with evaporation to clean and dry wafers. Wafers with tall bump features can trap fluid due to surface tension making drying more difficult. We have developed a model for fluid flow through a network of bumps. The model predicts that the fluid height between bumps will initially decrease rapidly and then much more slowly. Our model is in general agreement with our STG drying results, in which wafers with bumps taller than 30um require various amount of post-evaporative drying. Although our model predicts continued slow flow, in practice local non-uniformities will cause locally separated flow which will leave some areas with trapped fluid. A method to measure the local trapped fluid height, which will allow more quantitative comparisons with theory is shown in Fig. 7. The method uses a Zygo NewView 7300 Optical Surface Profiler and a controlled temperature support prevent evaporation or condensation.

References

[1] R.B. Bird, W.E. Stewart and E.N. Lightfoot, *Transport Phenomena* 2nd ed. (Wiley, New York, 2007) Chap. 6, pp. 178-188.

[2] H. Lamb Phil.Mag. (6) 21, 112 (1911)

[3] S.C.R. Dennis and M. Shimshoni, *The Steady Flow of a Viscous Fluid past a Circular Cylinder*(Her Magesty's Stationary Office, London 1965).

[4] N.A. Mortensen, F. Okkels and H. Bruss, Phys. Rev. E **71**, 057301 (2005).

[5] X. Fanton, A.M. Cazabat and D. Quere, Langmuir **12**, 5875-5880 (1996).

[6] M. Sobhian, A. Keigler and D. Goodman, "High-Speed Removal of Thick Negative Photoresist in Advanced Packaging Applications" in *Proceedings of the 10th Annual IWLPC Conference* (San Jose, CA., 2013)